Non-linear retreat of Jakobshavn Isbræ since the Little Ice Age controlled by geometry

Nadine Steiger[1], Kerim H. Nisancioglu[2,3], Henning Åkesson[2], Basile de Fleurian[2], and Faezeh M. Nick[4]

[1]Geophysical Institute, University of Bergen and the Bjerknes Centre for Climate Research, Bergen, Norway
[2]Department of Earth Science, University of Bergen and the Bjerknes Centre for Climate Research, Bergen, Norway
[3]Centre for Earth Evolution and Dynamics, University of Oslo, Oslo, Norway
[4]University Centre in Svalbard, Longyearbyen, Norway

Correspondence to: N. Steiger (nadine.steiger@uib.no)

Abstract. Rapid retreat of Greenland's marine-terminating glaciers coincides with the recent observed warming trend, which has broadly been used to explain rapid changes. However, Greenland glaciers within similar climate regimes experience widely contrasting retreat patterns, suggesting that the local fjord geometry could be important. To assess the relative role of climate and fjord geometry, we use the retreat history of Jakobshavn Isbræ, West Greenland, since the Little Ice Age maximum in 1850 as a baseline for the parametrization of a width-depth integrated ice flow model. The impact of fjord geometry is isolated by using a linearly increasing climate forcing and a range of simplified geometries.

We find that the strength of the retreat is determined by external factors—such as hydrofracturing, submarine melt and buttressing by sea ice—whereas the retreat pattern is governed by the fjord geometry. Narrow and shallow areas provide stabilization points and cause delayed rapid retreat after decades of grounding line stabilization without additional climate warming. We suggest that these geometric pinning points may be used as a proxy for moraine build-up and to predict the long term response of the glacier. As a consequence, to assess the impact of climate on the retreat history of a glacier, each system has to be analyzed with knowledge of its historic retreat and the local fjord geometry.

1 Introduction

Marine-terminating glaciers export ice from the interior of the Greenland Ice Sheet (GrIS) through deep troughs terminating in fjords (Joughin et al., 2017). Ice discharge accounts for about half of the current GrIS mass loss (Khan et al., 2015) and is impacted by several processes linked to air and ocean temperatures, of which most are poorly understood as well as spatially and temporally heavily undersampled (e.g. Straneo et al., 2013; Straneo and Cenedese, 2015). A warmer atmosphere enhances surface runoff, which may change the rheology and might cause crevasses to penetrate deeper through hydrofracturing, which in turn can promote iceberg calving (Benn et al., 2007; van der Veen, 2007; Cook et al., 2012, 2014; Pollard et al., 2015). A warmer ocean strengthens submarine melt below ice shelves and floating tongues (Holland et al., 2008a, b; Motyka et al., 2011), which can potentially destabilize the glacier through longitudinal dynamic coupling and upstream propagation of thinning (Nick et al., 2009; Felikson et al., 2017). Increased air and fjord temperatures can additionally weaken sea ice and ice mélange in fjords, affecting calving through altering the stress balance at the glacier front (Amundson et al., 2010; Robel, 2017).

Although observed acceleration and retreat around the GrIS is broadly associated with large-scale atmospheric and oceanic warming (e.g. Carr et al., 2013; Straneo et al., 2013), inland mass loss can be restricted by glacier geometry (Felikson et al., 2017). Despite widespread acceleration, individual glaciers correlate poorly with regional trends (Moon et al., 2012; Csatho et al., 2014): only four glaciers have accounted for 50 % of dynamic mass loss since 2000, where Jakobshavn Isbræ (JI) in West Greenland has been the largest contributor (Enderlin et al., 2014). These heterogeneous patterns are poorly understood, inhibiting robust projections of sea level rise from marine ice sheet loss. Attribution of observed changes also remains challenging because the relatively short period of observational records inhibits the understanding of the response of marine-terminating glaciers to external forcing. Here, we therefore use an expanded data set of climatic conditions reaching from the Little Ice Age (LIA) maximum in 1850 to present-day.

Compared to previous studies, our focus on a longer time period provides context for recent observed changes on JI in West Greenland. Since the deglaciation of Disko Bugt between 10.5–10.0 thousand years before present (kyr BP) (Ingólfsson et al., 1990; Long et al., 2003), JI has experienced an alteration between fast retreat and periods of stabilization, that formed large moraine systems (e.g. at Isfjeldsbanken, Fig. 1; Weidick and Bennike, 2007). Most observations exist after the Little Ice Age (LIA) maximum in 1850 (Fig. 1), when the glacier started retreating again and accelerated significantly after the disintegration of its 15 km long floating tongue from 2001 until May 2003 (Thomas et al., 2003; Joughin et al., 2004; Luckman and Murray, 2005; Motyka et al., 2011). It is now the fastest glacier on Greenland (Rignot and Mouginot, 2012) with a maximum velocity of $18\,\mathrm{km\,yr^{-1}}$ (measured in summer 2012; Joughin et al., 2014) and ice discharge rates of about 27–50 $\mathrm{km^3\,yr^{-1}}$ (Joughin et al., 2004; Rignot and Kanagaratnam, 2006; Howat et al., 2011; Cassotto et al., 2015). JI alone contributed to 4 % of the global sea level rise in the 20th century (IPCC, 2001) and is the glacier in Greenland with the largest contribution to sea level rise (Enderlin et al., 2014). It is also one of the most vulnerable glaciers in Greenland, with recent thinning potentially propagating as far inland as one third of the distance across the entire ice sheet (Felikson et al., 2017).

The recent rapid retreat of JI and other marine-terminating glaciers has been explained by regional warming (Holland et al., 2008a; Lloyd et al., 2011; Vieli and Nick, 2011; Carr et al., 2013; Straneo and Heimbach, 2013; Pollard et al., 2015). However, the dependence of ice discharge and marine ice sheet stability on the bed topography implies different responses of individual glaciers, even if exposed to the same climate (Warren, 1991; Moon et al., 2012). It is well-known that grounding line stability is highly dependent on trough geometry, with retrograde glacier beds potentially causing unstable, irreversible retreat (e.g. Schoof, 2007). The impact of glacier width is less studied, but lateral buttressing (Gudmundsson et al., 2012; Schoof et al., 2017) and topographic bottlenecks (Jamieson et al., 2012; Enderlin et al., 2013b; Jamieson et al., 2014) are suggested to stabilize grounding lines on reverse bedrock slopes. Despite these studies showing the importance of geometry, limited knowledge still exists regarding the interplay between bedrock geometry, channel-width variations and external controls on a real glacier. Most of the above mentioned studies on the control of geometry only focus on synthetic glaciers, prohibiting a model validation and justification of parameters choice. Also, there is still a strong emphasis in the community on the role of ice-ocean interactions as a key control on the retreat of marine-terminating glaciers (e.g. Holland et al., 2008a; Joughin et al., 2012; Straneo and Heimbach, 2013; Fürst et al., 2015; Cook et al., 2016).

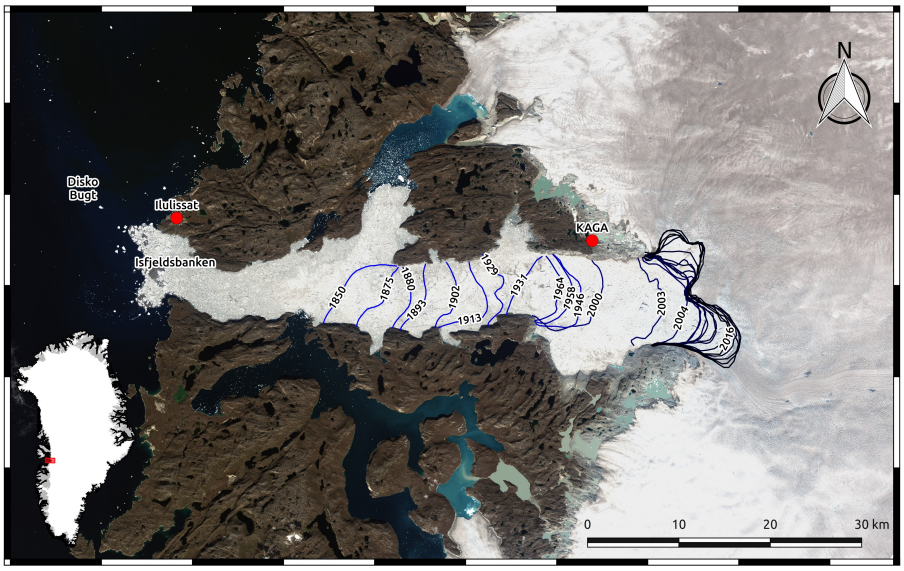

Figure 1. Glacier front positions of JI from Khan et al. (2015) (1850–1985) and CCI products derived from ERS, Sentinel-1 and LANDSAT data by ENVO (1990–2016). The background map is a LANDSAT-8 image from 16 August 2016 (from the U.S. Geological Survey). Location names that occur in the text are marked. The inset shows the location of JI on Greenland.

The aim of this study is to investigate the external, glaciological and geometric controls on JI in response to a linear forcing on a long time scale. We use a simple numerical ice flow model (e.g. Vieli et al., 2001; Nick et al., 2010) to assess the relative impact of geometry and climate forcing on the retreat of JI from the LIA maximum to present-day. Geometric controls are isolated (a) using a linear forcing to avoid complex responses and (b) artificially straightening the trough width and depth. The study extends to a centennial time scale to account for internal glacier adjustment. The application of the model on a real glacier provides a model validation against observed velocities and front positions, but also ensures the use of right dimensions for the width-depth ratio, velocities, and model parameters.

In Sect. 2 of this paper, the numerical ice flow model is described followed by Sect. 3 which describes the specific setup used for the simulations. In Sect. 4, the results of the forcing and geometry experiments are presented. Section 5 stresses the importance of the geometry compared to climate and discusses the resulting implication for geomorphology and the limitations of the model.

2 Modelling approach

A width and depth integrated flowline model (Nick et al., 2010) is used for this study. It benefits from a robust treatment of the grounding line, an explicit physical representation of the calving front, and is more efficient than complex models (Muresan

et al., 2016; Bondzio et al., 2016), which enables many model runs and the coverage of a centennial time scale. The used physical calving law has the advantage of allowing for a dynamic and free migration of the glacier terminus given changes in climate forcing. The climate forcing is implemented as a change in surface mass balance, crevasse water depth, submarine melt and buttressing by sea ice—parameters that are linked to temperature. In this section, the physical approach, parameterizations and the implementation of climate forcing are described.

2.1 Numerical ice flow model

The here used width and depth integrated numerical ice flow model is constructed for marine-terminating glaciers (Vieli et al., 2001; Vieli and Payne, 2005; Nick et al., 2009, 2010). Ice thickness variations with time are calculated from the along-flow ice flux and mass balance, using a width- and depth integrated continuity equation (Eq. 1).

$$\frac{\partial H}{\partial t} = -\frac{1}{W}\frac{\partial (HUW)}{\partial x} + \dot{B} \tag{1}$$

H is thereby the ice thickness, W the width, U the velocity and x the along-flow component. The mass balance $\dot{B}$ includes the surface mass balance (SMB) and submarine melt described in Sect. 2.3.

The ice flux is controlled by a balance of lateral and basal resistance, along-flow longitudinal stress gradient and driving stress (Eq. 2). Lateral resistance is parametrized using a width-integrated horizontal shear stress (van der Veen and Whillans, 1996) and we use a Weertman-type basal sliding law based on effective pressure (Fowler, 2010). The longitudinal stress gradient is dependent on the effective viscosity ν, which is non-linearly dependent on the strain rate and the rate factor (Nick et al., 2010).

$$2\frac{\partial}{\partial x}\left(H\nu\frac{\partial U}{\partial x}\right) - A_s\left[\left(H-\frac{\rho_w}{\rho_i}D\right)U\right]^{1/m} - \frac{2H}{W}\left(\frac{5U}{E_{lat}AW}\right)^{1/n} = \rho_i g H\frac{\partial s}{\partial x} \tag{2}$$

where s is the surface elevation, g the gravitational acceleration, D is the depth of the glacier below sea level, ρ_i and ρ_w are the densities of ice and ocean water, respectively. A is the rate factor and n and m are the exponents for Glen's flow law and sliding relations, respectively. The lateral enhancement factor E_{lat} is used to tune the lateral resistance and the basal sliding parameter A_s tunes the resistance from the bed.

The grounding line position is calculated with a flotation criterion based on hydrostatic balance (van der Veen, 1996). Its treatment relies on a moving grid that adjusts freely to the new glacier length at each time step, continuously keeping a node at the calving front (Vieli and Payne, 2005; Nick et al., 2009, 2010). This allows for a precise simulation of the glacier front and grounding line position using high grid resolution. The grid size is set to Δx = 300 m initially, which decreases further as the glacier retreats and the length decreases. At the marine terminus, a dynamic crevasse-depth calving criterion is used and further explained in Sect. 2.2.

2.2 Calving law

The here used fully-dynamic crevasse-depth criterion calculates calving where the sum of surface and basal crevasse depth (d_{sc} and d_{bc}) penetrate the whole glacier thickness (Nick et al., 2010). The depth of basal crevasses is calculated from tensile

Table 1. List of variables, physical parameters and constants used in the model. Values for the initial (LIA) forcing parameters are given in the lower part. Parameter values used for the glacier retreat experiments are listed in Table 2.

Symbol	Definition	Value	Unit
H	glacier thickness		m
t	time		yr
W	glacier width		m
x	along-glacier coordinate		m
U	velocity		$\mathrm{m\,yr^{-1}}$
B	mass balance		$\mathrm{m\,yr^{-1}}$
ν	viscosity		$\mathrm{Pa\,yr}$
D	depth below sea level		m
s	surface elevation		m
d_{bc}	depth of basal crevasses		m
d_{sc}	depth of surface crevasses		m
R_{xx}	tensile deviatoric stress		Pa
$\dot{\epsilon_{xx}}$	longitudinal strain rate		$\mathrm{m\,yr^{-2}}$
Q_L	lateral ice flux		$\mathrm{m\,yr^{-1}}$
a	surface mass balance (SMB)		$\mathrm{m\,yr^{-1}}$
g	gravitational acceleration	9.8	$\mathrm{m\,yr^{-1}}$
ρ_i	ice density	900	$\mathrm{kg\,m^{-3}}$
ρ_w	ocean water density	1028	$\mathrm{kg\,m^{-3}}$
ρ_{fw}	fresh water density	1000	$\mathrm{kg\,m^{-3}}$
m	sliding exponent	3	
n	Glen's flow law exponent	3	
A	rate factor taken from	A(-20°C) –	$\mathrm{yr^{-1}\,Pa^{-3}}$
	Cuffey and Paterson (2010)	A(-5°C)	
A_s	basal resistance parameter	120	$\mathrm{Pa\,m^{-2/m}\,s^{-1/m}}$
E_{lat}	lateral enhancement	10	
dx	grid size	250–300	m
dt	time step	0.005	yr
Perturbation parameters with their initial LIA values			
m	submarine melt rate	175	$\mathrm{m\,yr^{-1}}$
d_{cw}	crevasse water depth	160	m
G_{a1}	lower SMB gradient	0.0011	$\mathrm{m\,yr^{-1}}$
G_{a2}	upper SMB gradient	-0.002	$\mathrm{m\,yr^{-1}}$
a_0	maximal SMB	0.64	$\mathrm{m\,w.e.\,yr^{-1}}$
f_{si}	sea ice buttressing	1	

deviatoric stresses (R_{xx}) and the height above buoyancy. The depth of surface crevasses is caused by tensile deviatoric stresses and enhanced by melt water filling up crevasses due to the additional water pressure (Eq. 3; Nye, 1957; Nick et al., 2013). The

water depth in crevasses (d_{cw}) links calving rates to climate and is in our experiments used as a perturbation parameter.

$$d_{sc} = \frac{R_{xx}}{\rho_i g} + \frac{\rho_{fw}}{\rho_i} d_{cw}, \text{ with } R_{xx} = 2\left(\frac{\dot{\epsilon}_{xx}}{A}\right)^{1/n}, \tag{3}$$

where ρ_{fw} is the densities of freshwater. The tensile deviatoric stress R_{xx} is the difference between tensile stresses that pulls a fracture open and the ice overburden pressure. It is calculated from the longitudinal strain rate $\dot{\epsilon}_{xx}$ through Glen's flow law (Eq. 4).

Buttressing by sea ice is implemented as a sea ice factor (f_{si}), which can be reduced accounting for weakening of ice mélange by increasing the strain rate. The strain rate (Eq. 4) is responsible for the opening and downward-penetration of crevasses at the glacier terminus, consequently increasing calving rates.

$$\dot{\epsilon}_{xx} = \frac{\partial U}{\partial x} = f_{si} A \left[\frac{\rho_i g}{4}\left(H - \frac{\rho_w}{\rho_i}\frac{D^2}{H}\right)\right]^n \tag{4}$$

The model uses separate parameters for water in crevasses and sea ice buttressing, although they both impact the glacier response similarly by changing the calving rate. This separation is done because the two parameters are linked to different processes and can hence be forced separately.

2.3 Atmospheric and ocean forcing

The model SMB (a) is derived from observed monthly mean SMB data at JI (Box, 2013). Our implementation consists of a piecewise linear function of the surface elevation separated in two regions: the steep lower part below the transition height s_0 where the SMB increases with elevation and the higher surface elevations with low precipitation where the SMB decreases with elevation (Eq. 5).

$$a(x) = \left(a_0 - \frac{da}{dx}\cdot s_0\right) + \frac{da}{dx}\cdot s(x); \text{ with } \frac{da}{dx} = \begin{cases} G_{a1} & \text{for } s(x) \leq s_0 \\ G_{a2} & \text{for } s(x) > s_0 \end{cases} \tag{5}$$

Table 1 provides the LIA values (1840–1850 average) for the vertical gradients G_{a1} and G_{a2} as well as the SMB a_0 at the height s_0.

Submarine melt is implemented in the model as a vertical melt rate that reduces the ice thickness of the floating tongue. In this model, an along-tongue variation of submarine melt shows similar results to a constant submarine melt along the whole tongue, so that a spatially constant value is used here.

2.4 Lateral ice flow

Additionally to the SMB, the glacier is fed by tributary glaciers mainly adding mass in the lowermost 80 km. The formulation of those tributary ice flow is inspired by Lea et al. (2014) and based on mass conservation. The lateral influx Q_L is initially calculated at each grid point as the sum of the northern and southern lateral fluxes given by observed velocity ($U_{L,0}$) and thickness ($H_{L,0}$) (Rignot and Mouginot, 2012; Morlighem et al., 2014) weighted with the width of the main trough W_{JI}

(Eq. 6). This influx locally accounts to about 100 times the SMB, with a maximum of $120\,\mathrm{m\,yr^{-1}}$ (Fig. 2). Throughout the simulations, the lateral flux is parametrized to show the same evolution than the one of the main trunk and keep its relative contribution to the overall flux (Eq. 7).

$$Q_{L,0}(x) = \frac{U_{L,0}(x) \cdot H_{L,0}(x)}{W_{JI}(x)} \tag{6}$$

$$Q_{L,t}(x) = Q_{L,0}(x) \cdot \frac{Q_{JI,t}(x)}{Q_{JI,0}(x)} \tag{7}$$

3 Model setup

Despite the general focus of this study on the external versus geometric controls of glacier retreat, we apply the model to JI—a real glacier. The intension thereby is the use of a realistic along-glacier geometry and forcing. In addition, the total retreat of JI since the LIA is used for model tuning. For the initialization, observed trough geometry data are used (Boghosian et al., 2015) as well as the glacier extent during the LIA maximum (1850) (Khan et al., 2015). Observed velocities, ice thickness and ice discharge are used to tune parameters (Joughin et al., 2014; Howat et al., 2014; Joughin et al., 2004). For the model experiments, climate-related parameters are perturbed linearly to simulate increasing temperatures. During the retreat, the calving front and grounding line evolve freely with a total retreat rate depending on the forcing. Only those combinations of forcing parameters are considered, where the total glacier retreat corresponds to the observed 43 km from the LIA to 2015. In the following, the initial parameters and their perturbations are elucidated together with related observations.

3.1 Model initialization

We use a one-dimensional along-flow bed topography profile in the deep trough and fjord as it is presented in Boghosian et al. (2015). The fjord bathymetry is thereby obtained from Operation IceBridge gravity data and for the subglacial trough the profile from high-sensitivity radar data by Gogineni et al. (2014) are used here. For the bed upstream of the deep trough (77 km from the 2015 front position), 150 m resolution data by Morlighem et al. (2014) are averaged over the glacier width. The glacier width is defined as the trough width at the present-day sea level from topography data (Morlighem et al., 2014) and satellite images in the ice-free fjord (Fig. 1). JI's catchment widens gradually over the upper 445 km up to the ice divide, and the width is defined accordingly following Nick et al. (2013).

Basal sliding—as implemented in the model—changes the surface slope and hence the ice thickness at the ice divide. The basal sliding parameter $A_s = 120\,\mathrm{Pa\,m^{-2/3}\,s^{-1/m}}$ is therefore chosen for the LIA to achieve an observed present-day thickness of 3065 m at the ice divide (Howat et al., 2014); the present-day thickness in the interior can be used because the ice sheet is assumed to be in steady-state above 2000 m of elevation (Krabill, 2000). Also the height of the trimline found at the GPS station KAGA (Fig. 1; Jeffries, 2014) by Csatho et al. (2008) is used as a reference height. The impact of increased melt on basal sliding on interannual time scales is still unclear (Sole et al., 2011; Tedstone et al., 2015), so that the basal sliding parameter is kept constant in time and space in our model simulations. The strength of basal resistance of JI is highly debated

with some studies explaining high surface velocities with a slippery bed (Lüthi et al., 2002; Shapero et al., 2016; Bondzio et al., 2017), whereas other studies use weakened shear margins as explanation for high velocities (e.g. **?**).

The glacier surface is in addition determined by the lateral resistance and the rate factor. A constant lateral enhancement factor of $E_{lat} = 10$ is applied along the glacier that controls the strength of the transmission of lateral drag to the sides to achieve a present-day surface corresponding to observations (Howat et al., 2014). The rate factor for Glen's flow law is in a first approximation a function of ice temperature and here set to values corresponding to temperatures of -20°C at the ice divide linearly increasing to -5°C at the terminus (Cuffey and Paterson, 2010), which provides present day glacier surface and velocities closest to observations (Howat et al., 2014; Joughin et al., 2014). The rate factor is here kept temporally constant.

The depth of water filling crevasses has not been measured yet, but the chosen value of 160 m for the steady-state achieves the observed glacier length and a calving rate of 34 $\mathrm{km^3\,yr^{-1}}$ in 1985, which is in the same order of magnitude as the observed calving rate of 26.5 $\mathrm{km^3\,yr^{-1}}$ in 1985 (Joughin et al., 2004) and values obtained from other studies (24–50 $\mathrm{km^3\,yr^{-1}}$; Rignot and Kanagaratnam, 2006; Howat et al., 2011; Cassotto et al., 2015). The crevasse water depth may be exaggerated, as no submarine melt is applied at the vertical glacier front in the model and mass has to be removed.

3.2 Forcing experiments

A retreat of the initial LIA glacier is forced with simultaneous linear changes in SMB, crevasse water depth, submarine melt rate and sea ice buttressing. The parameter perturbations are thereby combined to force a total retreat of 43 km from 1850 to 2015, corresponding to the observed retreat. Nine different combinations are presented here that cover a wide range of perturbations for each parameter. The SMB is well known (Box, 2013), and all runs are therefore forced with the same gradual change in the SMB profiles. Table 2 shows the values that each parameter reaches in 2015 for the nine different model runs.

Sea ice buttressing can be assumed to decrease with increasing air and ocean temperatures, largely influencing iceberg calving (e.g. Sohn et al., 1998; Reeh et al., 2001). However, the correlation is poorly known and a temperature increase may only impact seasonal frontal migration, leaving annual fluxes unaffected (Amundson et al., 2010; Cassotto et al., 2015). We conduct experiments with unchanged sea ice buttressing ($f_{si} = 1$) as well as decreased buttressing by a factor two and three compared to the LIA value in 2015.

Submarine melt is influenced by ocean temperatures, which have increased from about 1.5 °C in 1980 to 3 °C in 2010 outside JI (Lloyd et al., 2011) with a 1 °C warming only in 1997 (Holland et al., 2008a; Hansen et al., 2012). Jenkins (2011) estimates about a doubling of melt rates underneath the tongue of JI depending on initial conditions and the way in which melting is applied, when considering a 1 °C warming and steepening of the glacier front. Submarine melt rates may additionally be enhanced by increased subglacial ice discharge (Jenkins, 2011; Xu et al., 2012, 2013; Sciascia et al., 2013), although this may be a local effect and negligible when with-averaged (Cowton et al., 2015). Since submarine melt rate is poorly constrained especially further back in time, we conduct a large range of linear forcing, from no increase, to a two fold increase of the LIA value reaching then 340 $\mathrm{m\,yr^{-1}}$ in 2015.

The increase in crevasse water depth is unknown, but may be comparable to the increase in runoff, which has increased by 63 % since the LIA (Box, 2013). To account for a large range, we increase the crevasse water depth from its LIA value depths

Table 2. Nine combinations of the perturbation parameters used in this study. Values shown here are those reached in 2015 after a linear perturbation from their LIA value shown in Table 1. Values for the SMB are perturbed to the same 2015-values for all model runs: $G_{a1} = 0.0019\,\mathrm{yr}^{-1}$, $G_{a2} = -0.00013\,\mathrm{yr}^{-1}$, $a_0 = 0.64\,\mathrm{m\,w.e.\,yr}^{-1}$. Run 5 (in bold) is presented in more detail in the paper.

run ID	f_{si}	m $[\mathrm{m\,yr}^{-1}]$	c_{cw} [m]
2015 value reached through linear forcing			
1	1	180	395
2	1	260	370
3	1	340	340
4	2	180	295
5	**2**	**260**	**275**
6	2	340	255
7	3	180	225
8	3	260	210
9	3	340	185
step forcing applied in year 1850			
10	2	260	250

between 185 m and 395 m in 2015. It is thereby tuned depending on the combination of sea ice buttressing and submarine melt rate to reach the observed retreat (Table 2).

In order to reach the same total retreat in all combinations presented in Table 2, the 2015-values for each parameter depend on the values for the other parameters. This means e.g. that a high submarine melt rate is needed in case of reduced sea ice buttressing and a small crevasse water depth or that the crevasse water depth has to be large when sea ice buttressing is not reduced and the submarine melt rate small.

In addition to experiments with linearly increased parameters, we also conduct one experiment with a step increase in the three parameters after the LIA maximum. The values are comparable to run 5, with slightly different values to reach the right front position in 2015. All experiments shown in Table 2 are run until 2100 to expand the temporal and spatial dimensions to show the importance of the geometry.

Despite a relatively high amount of frontal observations since the LIA (Fig. 1), only the observed calving front positions in 1850 and 2015 are used here to tune the parameters; in between, the forcing parameters increase linearly and the glacier length evolves freely. Nevertheless, we present the time evolution of the simulated front positions together with observations. To obtain one-dimensional observed front positions, we first calculate a centerline as a smoothed line following the mean latitudinal position of each observed glacier front (Fig. 1). The front positions are then chosen where the observed calving

fronts intersect with the model centerline; the uncertainty of the front positions is calculated as the maximal spread of each front in cross-trough direction.

3.3 Geometric experiments

In addition to the effect of forcing, we also test the impact of fjord geometry on glacier retreat. We design experiments with a smoothed width and depth in the deep and narrow trough. Four different geometry combinations are constructed and shown in Fig. 2.

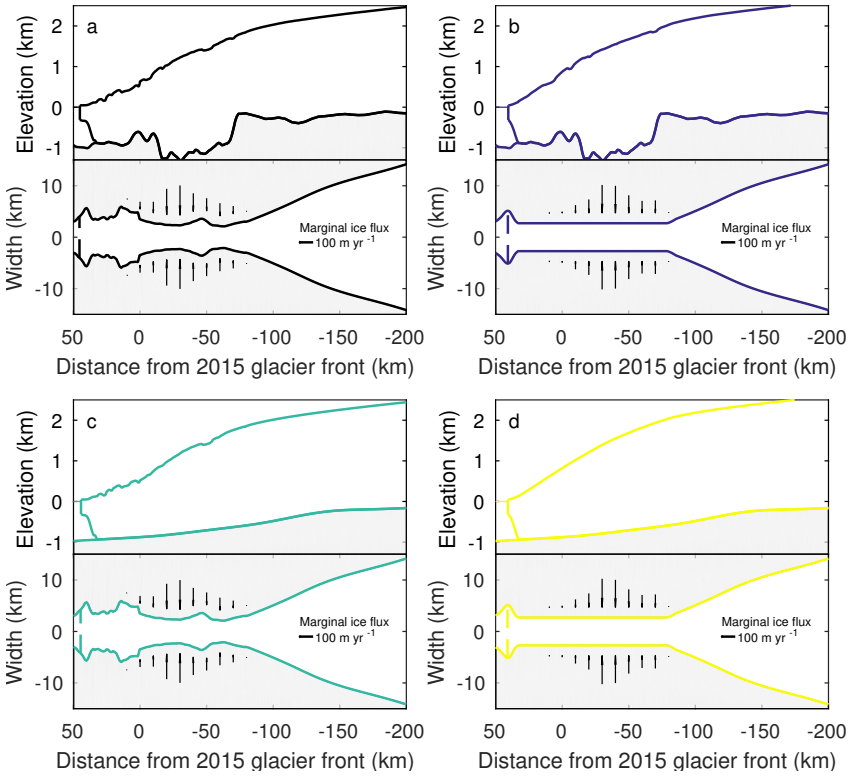

Figure 2. Different model geometries used to investigate the impact of topography on ice dynamics. (a) Original geometry, (b) straight width, (c) straight bed and (d) straight width and bed. Arrows indicate the tributary ice flux, with their length representative for the influx volume.

a Original geometry: Observed width and depth of the trough as described in Sect. 3.1.

b Straight width: The width until 80 km inland of today's front is set to a constant value of 5.4 km. Only at the LIA front position, a wide section is kept in order to reach a steady-state with the same parameters. The depth is kept as in **a**.

c Straight bed: The bed of the deep trough to 120 km inland of today's front is smoothed to get an almost straight bed, linearly rising inland. The width is kept as in **a**.

d Straight width and bed: Both, the width and the bed are straightened here.

The runs with simplified geometry start from steady-state at the LIA front position with the same parameters and forcing as for the original model setup (Table 2). Due to the changed topographies, the glacier surfaces and velocities differ from the original geometry and the LIA front position is slightly changed.

4 Results

In this section, we present the steady-state glacier at the LIA maximum extent and the glacier retreat simulated with run 5 (Table 2) as an example. In addition, the response to different forcing parameter combinations, more simplified geometries and a step forcing is presented.

4.1 Jakobshavn Isbræ at the LIA maximum

The initial steady-state glacier as shown in Fig. 2a and 4a is reached with the parameters in Table 2. It has an uneven surface that reflects the trough geometry, which is common for fast flowing ice streams (Gudmundsson, 2003). At the position of KAGA, the surface elevation is about 400 m compared to the 300 m of the LIA-trimline height Csatho et al. (2008); however, the side margins are expected to be lower than the centerline and the model glacier has a—probably overestimated—surface bump at that position. The LIA glacier terminates with a 9 km long floating tongue, where it has a velocity of $5\,\mathrm{km\,yr^{-1}}$ and a grounding line flux of $35\,\mathrm{km\,yr^{-1}}$. The modelled width-averaged basal shear stress is about 128 kPa at 40 km inland of the present-day front position and the driving stress is 290 kPa at that location, when applying a 3 km moving average to smooth the surface bumps. Compared to this, ice flow simulations suggest low basal resistance (Joughin et al., 2012; Habermann et al., 2013) and data assimilation methods imply basal stresses at the bed of the deep trough of about 65 kPa at 50 km upstream of the calving front, equivalent to only 20 % of the driving stress (Shapero et al., 2016).

4.2 Non-linear glacier response to linear forcing

Figures 3 a,b show that the modelled front position retreats non-linearly in response to the linear external forcing (shown here is run 5 in Table 2). It retreats 21 km during the first 163 years, after which a 16 km long floating tongue forms. During the break-off of the tongue in 2013 to 2014, the front retreats further 23 km. Throughout the retreat, the glacier terminus configuration alternates between a floating tongue and a grounded front. The front velocities (Fig. 3c) only increase by $3\,\mathrm{km\,yr^{-1}}$ during the first 163 years and more than double from $8\,\mathrm{km\,yr^{-1}}$ to $19\,\mathrm{km\,yr^{-1}}$ when the floating tongue breaks off. This acceleration is overestimated, as the simulated tongue breaks off faster than observed. However, velocity observations by Joughin et al. (2014), shown in Fig. 3c, are in-between the simulated velocities before and after the break-off. The model simulations show that the acceleration continues until the retreat of the front slows down. The grounding line flux, calculated as the grounding line velocity times the grounding line gate area, increases from $35\,\mathrm{km^3\,yr^{-1}}$ to $65\,\mathrm{km^3\,yr^{-1}}$ from the LIA until 2015. Beyond 2015 it increases to $100\,\mathrm{km^3\,yr^{-1}}$ and finally stabilizes with $77\,\mathrm{km^3\,yr^{-1}}$.

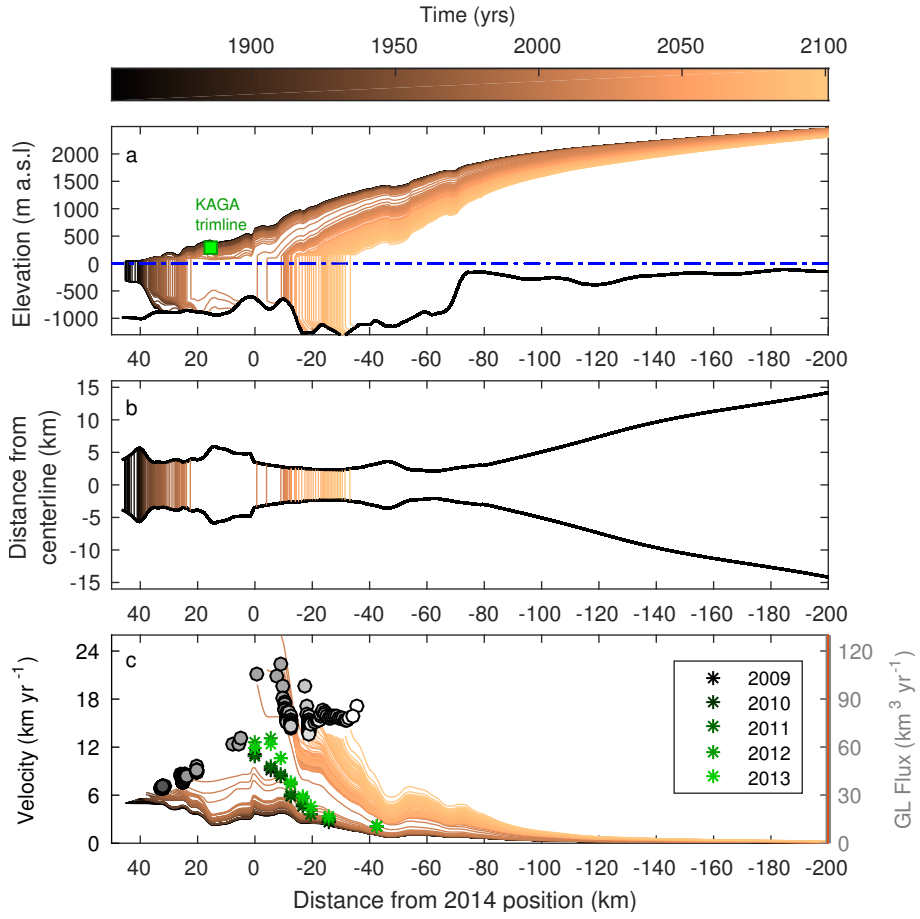

Figure 3. Modeled retreat of JI in response to a gradual change of the forcing parameters (run 5 in Table 2). Yearly profiles are shown for (a) the along-flow glacier profile and the elevation of the KAGA LIA trimline (Csatho et al., 2008) in green, (b) the front positions in a top-view and (c) the along-glacier annual velocities including the yearly grounding line (GL) flux (grey circles from dark to light with time) and observed yearly velocities at seven different points upstream from the glacier front from 2009 to 2013 (Joughin et al., 2014).

Various parameter combinations presented in Table 2—and many more that are approximately an interpolation of those presented here—force the observed total retreat since the LIA. Figure 4 shows the retreat of the glacier front and grounding line with time for the applied nine parameter combinations. The simulated evolution of the frontal position is similar for all experiments and shows the strong non-linearity of the frontal retreat—despite the linear forcing (Fig. 4a). The response to the different forcing experiments differs mainly in the timing of each further retreat, especially the final retreat just after 2050. All model runs show a very abrupt retreat of at least 23 km within a few years, which corresponds to the observed retreat of 19 km after year 2000. The simulated frontal positions from the observations, but due to the simplicity of the model and the forcing, the aim is here to study the geometric controls on rapid retreat rather than tuning the model until the simulated retreat fits the observations. The deviation of the simulations from the observations is discussed in Sect. 5.

The grounding line retreats more step-wise (Fig. 4b) compared to the glacier front. Before 2015, it stabilizes at distances of 32 km, 25 km and 20 km from the 2015 frontal position for all experiments. It retreats more gradually beyond 2015 with short stabilizations at 8 km, 12 km and 18 km upstream of the present-day position. The parameter combination thereby only determines the timing of the grounding line displacement.

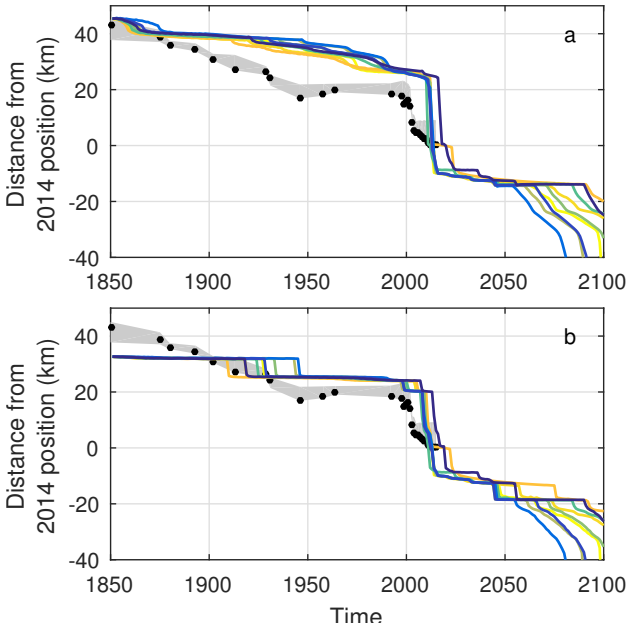

Figure 4. Simulated position of (a) the front and (b) the grounding line for nine different gradual forcing combinations presented in Table 2. The colors for the different model runs are random. Black dots show the observed front positions at the centreline with a spread corresponding to the across-fjord variation of each front position (Fig. 1).

4.3 Control of fjord geometry on grounding line retreat

The stability of the grounding line is analyzed here for the different geometries introduced in Fig. 2. Stability is thereby quantified by the time the grounding line rests at one position. Figure 5a shows the original geometry with the most pronounced pinning points at distances of 32 km, 25 km, -10 km and -13 km from the 2015 position. Only the length of stabilization thereby varies among the nine different model runs (Table 2), whereas the stabilization locations coincide (also seen in Fig. 4b). Artificially straightening the width removes the pinning points at 25 km and those beyond the 2015 position(Fig. 5b) . Instead, the glacier stabilizes at the present-day position. The geometry with the straightened bed causes a similar response to the linear forcing as the original geometry, only with a wider spread of stabilization points (Fig. 5c). Straightening the bed and the width removes all pinning points (Fig. 5d) and leads to a linear retreat. Note that all geometries have an initial pinning points at the LIA position to allow a steady-state at the LIA position. Generally, a reduction in the complexity of the fjord geometry, e.g. straightening the bed and/or width reduces the number of pinning points.

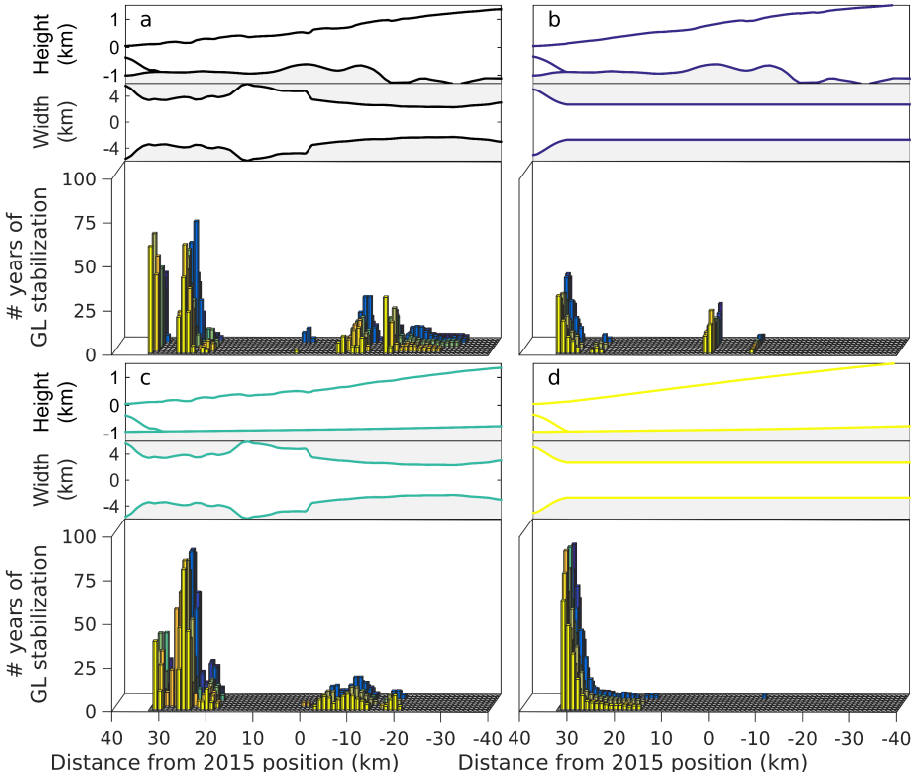

Figure 5. Stabilization of the grounding line (GL) for the different geometries presented in Sect. 3.3: (a) the original geometry, (b) straightened width, (c) straightened bed and (d) straightened width and bed. The bars represent the time that the grounding line rests within 1 km (in years), and the colours correspond to the model runs in Table 2. Only stable periods of more than two years are included.

4.4 Delayed abrupt glacier response

In addition to the linear increase in climate forcing, the response to a step forcing (Table 2) is presented in Fig. 6. With the step forcing, the glacier front remains stable at a distance of 22 km for 60 years, before it retreats rapidly to its new stable positions. This unprovoked rapid retreat—after centuries of constant forcing—demonstrates the long response time of the glacier (Nye, 1960; Jóhannesson et al., 1989; Bamber et al., 2007). The long response time is caused by a slow adjustment of the glacier volume to external changes. The corresponding accumulated volume loss also shown in Fig. 6 adjusts steadily to the initial changes in forcing, despite the stable grounding line. During the rapid front retreat, the volume decreases by 300 Gt and continues even after the grounding line stabilizes. This emphasized that a stable grounding line does not imply a steady-state. Similarly, an observed rapid retreat of a marine-terminating glacier might be the delayed response to previous temperature changes.

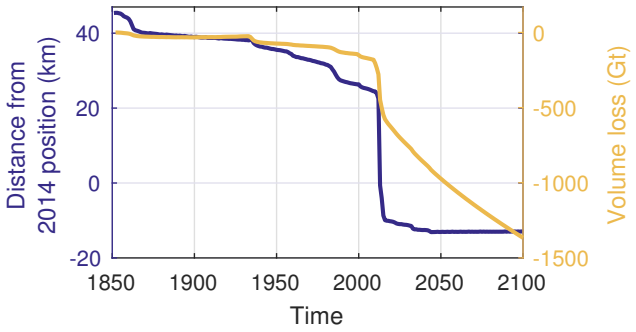

Figure 6. Simulated front positions and accumulated volume loss for the step forcing (Table 2).

5 Discussion

Our results show the importance of lateral and basal topography and its implications for the evolution of glacier retreat in fjords. JI on Greenland studied here is only one example. This challenges our understanding of the recent observed retreat history and makes it hard to isolate the relative impact of changes in ocean forcing, SMB and internal factors including the fjord geometry. Here, we discuss the impact of fjord geometry and compare the simulated glacier response to the recorded long term glacier retreat history, as well as explore the implications for the future response of JI to changes in climate.

We argue that fjord geometry to a large extent controls the retreat history of marine-terminating glaciers. Nevertheless, changes to the external forcing of the glacier are important as their magnitude times the onset of the retreat and determines its strength of the retreat (Fig. 4).

5.1 Geometric control on glacier stability

Our simulations show that once a glacier retreat is triggered through changes at the marine boundary or at the glacier surface, a non-linear response unfolds due to variations in the fjord geometry with a complexity given by the bed topography and the trough width.

For a retrograde bed, in a one-dimensional model, variations in the underlying bed topography influence the ice discharge, leading to an unstable glacial retreat (Weertman, 1974; Schoof, 2007). Previous studies also show that changes in the width of a glaciated fjord impact the lateral resistance, thereby stabilizing the glacier in narrow sections (Gudmundsson et al., 2012; Jamieson et al., 2012, 2014; Enderlin et al., 2013b; Morlighem et al., 2016). These findings are corroborated in our study. However, most of these studies use synthetic glaciers that do not allow for a validation of the model, they use a shorter time period that disregards long term adjustments or they use a realistic forcing that makes the role of the geometry nontransparent. Figure 6 shows that the time scale of glacier adjustment can be several decades long. However, in reality temperature does not change step-wise and it changes less than shown here. It still shows that the observed recent retreat can be the consequence of a warming that set in much earlier.

In Figure 5, the relative role of glacier width versus glacier length on JI is assessed. A flat glacier bed is less effective in reducing the non-linearity compared to straight lateral boundaries. It has to be considered that the glacier trough is an order of magnitude wider than it is deep with larger variations in the width compared to the bed, resulting in a larger importance of the glacier width. Whether this is the case in reality has to be studied further.

5.2 Relative role of forcing parameters

Only certain parameter combinations simulate the observed total retreat of JI since the LIA (Table 2). If the submarine melt rate is increased, the crevasse water depth has to be reduced and/or the sea ice buttressing increased. Similarly, if the sea ice buttressing is reduced, the crevasse water depth and submarine melt rate have to be smaller (Table 2). Importantly, none of the forcing parameters can trigger the retreat alone, given that they are perturbed within a reasonable range. Only changed individually, the submarine melt rate would have to reach $650\,\mathrm{m.yr^{-1}}$ in 2015—an increase by 370 % from the LIA, the crevasse water depth has to increase to 400 m (250 % of the LIA value), and the sea ice buttressing factor has to be 4.2 in 2015 to force a strong enough retreat. Absolute values for the parameters have to be taken with caution, because they do not necessarily correspond to physical variables. For example, to reach the observed grounding line flux, the value for the crevasse water depth is likely too high in our study. This is due to the lack of vertical submarine melt at the calving front in the model. The change in parameters required to trigger the retreat is also dependent on the initial parameter choices. As shown by Enderlin et al. (2013a), non-unique parameter combinations can exist for the same front positions, implying that real-world observations are vital to reduce uncertainty in transient model simulations.

Note that the SMB has an insignificant contribution to the frontal retreat, even if the frontal gradient is doubled and the SMB curve is lowered by 50 %, which together gives a SMB of -6 $\mathrm{m\,w.e.\,yr^{-1}}$ at the terminus compared to -1.1 $\mathrm{m\,w.e.\,yr^{-1}}$ during LIA. In the model and for this glacier, changes in air temperatures therefore contribute mainly through runoff and the filling of crevasses with water, rather than directly through surface ablation. For the specific geometry of JI, the influx of ice at the lateral boundaries is a factor 100 larger than the SMB and could be important for the sensitivity of the glacier to changes in climate forcing. However, the lateral flux has a minor impact on the retreat rate, and if all other parameters are kept fixed, the lateral influx has to be decreased by nearly 70 % to match the observed retreat, which is deemed unrealistic.

5.3 Model limitations

Although the model captures the observed rapid retreat after the disintegration of the floating tongue, neither the step forcing nor the linear forcing reproduce all the details of the observed retreat history since the LIA (Fig. 4 and Fig. 6). The magnitude of the rapid retreat is also exaggerated, which leads to an overestimation of the velocities, giving higher ice discharge compared to observations. However, a perfect match is not expected from a simple ice flow model as is used here, in particular given the linear forcing applied and the difficulty in measuring bed topography and bathymetry in this area (Boghosian et al., 2015). Due to the importance of the trough geometry, a small inaccuracy in the geometry would cause a different retreat.

If the objective is to accurately predict or reconstruct the time evolution of glacier retreat (e.g. Nick et al., 2013; Muresan et al., 2016; Bondzio et al., 2017), a more sophisticated model has to be used accounting for the following shortcomings in the one-dimensional model:

Bed topography is averaged over the width, which removes bumps in the trough that partly ground the floating part as it was observed by Thomas et al. (2003). The glacier width becomes symmetric due to the width-averaging, although in reality the trough can be widening on one side and narrowing on the other. This asymmetry causes an uneven frontal retreat as seen in Fig. 1. The bed and the lateral walls are treated as flat, which causes a stronger stabilization at pinning points. The depth and width integration also applies to internal glacier properties; ice temperatures are in reality high at the bottom (Lüthi et al., 2002), so that most deformation happens there, whereas the model assumes a vertically constant shearing and a constant rate factor. Along the glacier margins, ice viscosity drops significantly in response to acceleration and calving front migration (Bondzio et al., 2017) and marginal crevasses can form, which is disregarded. The lateral inflow from the surrounding ice is here changed with time depending on the ice flux in the main trough. This allows for a dynamic response of the lateral influxes, but to be more realistic, the whole catchment area should be included. In addition, calving and submarine melt rates could be included in a different way, although these processes are still poorly understood and a different submarine melt rate implementation barely contributes to the glacier behaviour as modelled here. Also, the model only outputs annual values for velocity, front position and calving fluxes, which should all be regarded interannually to account for seasonal changes that may have an impact on annual changes.

Note that also the observations contain uncertainties, as the front position can vary by several kilometers seasonally (e.g. Amundson et al., 2010) and the position varies by several kilometers across the trough (Fig. 1).

5.4 Predicting moraine positions

Figure 5 illustrates the potential in using the model simulations in a geomorphological context. Marine-terminating glaciers continuously erode their beds and deposit sediments, forming submarine landforms such as moraines. The rate of sediment deposition and resulting proglacial landforms are functions of climatic, geological and glaciological variables, though these functions remain poorly quantified due to sparse observational constraints. Proglacial transverse ridges tend to form during gradual grounded calving front retreat, whereas more pronounced grounding zone wedges are associated with episodic grounding line retreat (Dowdeswell et al., 2016).

The abundance of ice mélange in front of JI renders studies of submarine geomorphology difficult. Studies of this kind are lacking in the fjord, though evidence of the style of deglacial ice sheet retreat in Disko Bugt do exist (Streuff et al., 2017). Our study raises generic questions about the links between trough geometry and moraine positions. We suggest that moraine positions to a first order can be predicted from the glacier width, which here largely determines the position of grounding line stabilization. In this context, numerical models can be used to calculated the position and duration of stabilization from the glacier width as in Fig. 5, which then can be used as proxy for moraine build-up.

Thereby, stable (moraine) positions are independent of model parameters, supporting geometric controls of moraine formation. This hypothesis remains to be tested with a model including sediment dynamics and constrained by a number of

well-studied, diverse glaciological and climatic environments. While not a substitute for in-situ investigations, potential sites for more detailed (and costly) submarine studies could also be identified based on geometric information, using airborne or remotely sensed platforms. To this end, our study clearly highlights the potential of combing long-term modelling studies with geomorphological and sedimentary evidence to understand the non-linear response of marine ice sheet margins. This needs to be considered when inferring information on the climate by looking at glacier retreat reconstructions.

6 Conclusions

The rapid retreat of many of Greenland's outlet glaciers during the last decades has been correlated with increased oceanic and atmospheric temperatures, though glaciers display diverse behavior. We use the fjord geometry of JI as case study with a realistic setup of a numerical model forced with a linear increase in SMB, submarine melt rate, crevasse water depth and reduction in sea ice buttressing to isolate the importance of geometry for temporary grounding line stability. The following conclusions can be drawn:

- The glacier response to a linear climate forcing is highly non-linear.
- A change in climate forcing determines the strength and the timing of the glacier retreat; for our model glacier, SMB plays a negligible role and climate-related processes such as calving and submarine melt act together to cause the observed total retreat of JI.
- Fjord geometry determines the position of temporary grounding line stability; straightening the trough topography reduces the non-linearity of the glacier's retreat.
- Grounding line stabilization on pinning points can cause delayed rapid retreat due to a long adjustment to past changes in external forcing.

We argue that the retreat history of Jakobshavn Isbræ since the LIA has largely been controlled by changes in the trough width and depth and that future retreat will be governed by similar factors. Since grounding line stability is fundamentally controlled by the geometry, we also postulate that geometry—notably trough width—can be used to infer sites of moraine formation.

Code and data availability. The model code is available through Faezeh M. Nick (faezeh.nick@gmail.com). The model output and other datasets can be obtained upon request from the corresponding author.

Author contributions. Nadine Steiger, Kerim H. Nisancioglu and Henning Åkesson designed the research, Nadine Steiger performed the model runs and created the figures with significant input from Kerim H. Nisancioglu, Henning Åkesson and Basile de Fleurian. Faezeh Nick provided the model and technical support. Nadine Steiger wrote the paper, with substantial contributions from all authors.

Competing interests. The authors declare that they have no conflict of interest.

Acknowledgements. This research was funded by the Fast Track Initiative from Bjerknes Centre for Climate Research and the European Research Council under the European Community's Seventh Framework Programme (FP7/2007-2013)/ERC grant agreement 610055 as part of the ice2ice project. Henning Åkesson was supported by the Research Council of Norway (project no. 229788/E10), as part of the research project Eurasian Ice Sheet and Climate Interactions (EISCLIM). Front positions of JI since 1990 are obtained from ENVO at http://products.esa-icesheets-cci.org/. We want to thank Mahé Perrette for providing a python-javascript project to produce a 1-D profile of bed topography and glacier surface, which is available at https://github.com/perrette/webglacier1d. Thanks to Jason Box for providing SMB data for the GrIS. We also thank Martin Lüthi and Johannes Bondzio for constructive review that improved the manuscript greatly.

References

Amundson, J. M., Fahnestock, M., Truffer, M., Brown, J., Lüthi, M. P., and Motyka, R. J.: Ice mélange dynamics and implications for terminus stability, Jakobshavn Isbræ, Greenland, J. Geophys. Res-Earth, 115, 1–12, https://doi.org/10.1029/2009JF001405, 2010.

Bamber, J. L., Alley, R. B., and Joughin, I.: Rapid response of modern day ice sheets to external forcing, Earth Planet Sc. Lett., 257, 1–13, https://doi.org/10.1016/j.epsl.2007.03.005, 2007.

Benn, D. I., Warren, C. R., and Mottram, R. H.: Calving processes and the dynamics of calving glaciers, Earth-Sci. Rev., 82, 143–179, https://doi.org/10.1016/j.earscirev.2007.02.002, 2007.

Boghosian, A., Tinto, K., Cochran, J. R., Porter, D., Elieff, S., Burton, B. L., and Bell, R. E.: Resolving bathymetry from airborne gravity along Greenland fjords, J. Geophys. Res-Sol. Ea., 119, https://doi.org/10.1002/2014JB011381.Received, 2015.

Bondzio, J. H., Seroussi, H., Morlighem, M., Kleiner, T., Rückamp, M., Humbert, A., and Larour, E. Y.: Modelling calving front dynamics using a level-set method: application to Jakobshavn Isbræ, West Greenland, The Cryosphere, 10, 497–510, 2016.

Bondzio, J. H., Morlighem, M., Seroussi, H., Kleiner, T., Rückamp, M., Mouginot, J., Moon, T., Larour, E. Y., and Humbert, A.: The mechanisms behind Jakobshavn Isbræ's acceleration and mass loss: a 3D thermomechanical model study, Geophysical Research Letters, 2017.

Box, J. E.: Greenland ice sheet mass balance reconstruction. Part II: Surface mass balance (1840-2010), J. Climate, 26, 6974–6989, https://doi.org/10.1175/JCLI-D-12-00518.1, 2013.

Carr, J. R., Stokes, C. R., and Vieli, A.: Recent progress in understanding marine-terminating Arctic outlet glacier response to climatic and oceanic forcing: Twenty years of rapid change, Prog. Phys. Geog., 37, 436–467, https://doi.org/10.1177/0309133313483163, 2013.

Cassotto, R., Fahnestock, M., Amundson, J. M., Truffer, M., and Joughin, I.: Seasonal and interannual variations in ice melange and its impact on terminus stability, Jakobshavn Isbræ, Greenland, J. Glaciol., 61, 76–88, https://doi.org/10.3189/2015JoG13J235, 2015.

Cook, A., Holland, P., Meredith, M., Murray, T., Luckman, A., and Vaughan, D.: Ocean forcing of glacier retreat in the western Antarctic Peninsula, Science, 353, 283–286, 2016.

Cook, S., Zwinger, T., Rutt, I. C., O'Neel, S., and Murray, T.: Testing the effect of water in crevasses on a physically based calving model, Ann. Glaciol., 53, 90–96, https://doi.org/10.3189/2012AoG60A107, 2012.

Cook, S., Rutt, I. C., Murray, T., Luckman, a., Zwinger, T., Selmes, N., Goldsack, a., and James, T. D.: Modelling environmental influences on calving at Helheim Glacier in eastern Greenland, Cryosphere, 8, 827–841, https://doi.org/10.5194/tc-8-827-2014, 2014.

Cowton, T., Slater, D., Sole, A., Goldberg, D., and Nienow, P.: Modeling the impact of glacial runoff on fjord circulation and submarine melt rate using a new subgrid-scale parameterization for glacial plumes, J. Geophys. Res-Oceans, 120, 796–812, https://doi.org/10.1002/2014JC010324, 2015.

Csatho, B., Schenk, T., Van Der Veen, C. J., and Krabill, W. B.: Intermittent thinning of Jakobshavn Isbrae, West Greenland, since the Little Ice Age, J. Glaciol., 54, 131–144, https://doi.org/10.3189/002214308784409035, 2008.

Csatho, B. M., Schenk, A. F., van der Veen, C. J., Babonis, G., Duncan, K., Rezvanbehbahani, S., Van Den Broeke, M. R., Simonsen, S. B., Nagarajan, S., and van Angelen, J. H.: Laser altimetry reveals complex pattern of Greenland Ice Sheet dynamics, Proceedings of the National Academy of Sciences, 111, 18 478–18 483, 2014.

Cuffey, K. and Paterson, W.: The Physics of Glaciers, Butterworth-Heinemann/Elsevier, Burlington, MA, fourth edn., https://doi.org/10.1007/s13398-014-0173-7.2, 2010.

Dowdeswell, J., Canals, M., Jakobsson, M., Todd, B. J., Dowdeswell, E., and Hogan, K.: Atlas of submarine glacial landforms: Modern, Quaternary and Ancient, Geological Society of London, 2016.

Enderlin, E. M., Howat, I. M., and Vieli, A.: The sensitivity of flowline models of tidewater glaciers to parameter uncertainty, Cryosphere, 7, 1579–1590, https://doi.org/10.5194/tc-7-1579-2013, 2013a.

Enderlin, E. M., Howat, I. M., and Vieli, A.: High sensitivity of tidewater outlet glacier dynamics to shape, Cryosphere, 7, 1007–1015, https://doi.org/10.5194/tc-7-1007-2013, 2013b.

Enderlin, E. M., Howat, I. M., Jeong, S., Noh, M. J., Van Angelen, J. H., and Van Den Broeke, M. R.: An improved mass budget for the Greenland ice sheet, Geophys. Res. Lett., 41, 866–872, https://doi.org/10.1002/2013GL059010, 2014.

Felikson, D., Bartholomaus, T. C., Catania, G. A., Korsgaard, N. J., Kjær, K. H., Morlighem, M., Noël, B., van den Broeke, M., Stearns, L. A., Shroyer, E. L., Sutherland, D. A., and Nash, J. D.: Inland thinning on the Greenland ice sheet controlled by outlet glacier geometry, Nat. Geosci., 10, https://doi.org/10.1038/ngeo2934, 2017.

Fowler, A. C.: Weertman, Lliboutry and the development of sliding theory, J. Glaciol., 56, 965–972, https://doi.org/10.3189/002214311796406112, 2010.

Fürst, J., Goelzer, H., and Huybrechts, P.: Ice-dynamic projections of the Greenland ice sheet in response to atmospheric and oceanic warming, The Cryosphere, 9, 1039–1062, 2015.

Gogineni, S., Yan, J. B., Paden, J., Leuschen, C., Li, J., Rodriguez-Morales, F., Braaten, D., Purdon, K., Wang, Z., Liu, W., and Gauch, J.: Bed topography of Jakobshavn Isbræ, Greenland, and Byrd Glacier, Antarctica, J. Glaciol., 60, 813–833, https://doi.org/10.3189/2014JoG14J129, 2014.

Gudmundsson, G. H.: Transmission of basal variability to a glacier surface, J. Geopys. Res., 108, 1–19, https://doi.org/10.1029/2002JB002107, 2003.

Gudmundsson, G. H., Krug, J., Durand, G., Favier, L., and Gagliardini, O.: The stability of grounding lines on retrograde slopes, Cryosphere, 6, 1497–1505, https://doi.org/10.5194/tc-6-1497-2012, 2012.

Habermann, M., Truffer, M., and Maxwell, D.: Changing basal conditions during the speed-up of Jakobshavn Isbræ, Greenland, Cryosphere, 7, 1679–1692, https://doi.org/10.5194/tc-7-1679-2013, 2013.

Hansen, M. O., Gissel Nielsen, T., Stedmon, C. a., and Munk, P.: Oceanographic regime shift during 1997 in Disko Bay, Western Greenland, Limnol. Oceanogr., 57, 634–644, https://doi.org/10.4319/lo.2012.57.2.0634, 2012.

Holland, D. M., Thomas, R. H., de Young, B., Ribergaard, M. H., and Lyberth, B.: Acceleration of Jakobshavn Isbræ triggered by warm subsurface ocean waters, Nat. Geosci., 1, 659–664, https://doi.org/10.1038/ngeo316, 2008a.

Holland, P. R., Jenkins, A., and Holland, D. M.: The response of Ice shelf basal melting to variations in ocean temperature, J. Climate, 21, 2558–2572, https://doi.org/10.1175/2007JCLI1909.1, 2008b.

Howat, I. M., Ahn, Y., Joughin, I., Van Den Broeke, M. R., Lenaerts, J. T. M., and Smith, B.: Mass balance of Greenland's three largest outlet glaciers, 2000-2010, Geophys. Res. Lett., 38, 1–5, https://doi.org/10.1029/2011GL047565, 2011.

Howat, I. M., Negrete, A., and Smith, B. E.: The Greenland Ice Mapping Project (GIMP) land classification and surface elevation data sets, Cyrosphere, 8, 1509–1518, https://doi.org/10.5194/tc-8-1509-2014, 2014.

Ingölfsson, Ö., Frich, P., Funder, S., and Humlum, O.: Paleoclimatic implications of an early Holocene glacier advance on Disko Island, West Greenland, Boreas, 19, 297–311, https://doi.org/10.1111/j.1502-3885.1990.tb00133.x, 1990.

Jamieson, S. S., Vieli, A., Livingstone, S. J., Ó Cofaigh, C., Stokes, C., Hillenbrand, C.-D., and Dowdeswell, J. a.: Ice-stream stability on a reverse bed slope, Nat. Geosci., 5, 799–802, https://doi.org/10.1038/NGEO1600, 2012.

Jamieson, S. S. R., Vieli, A., Cofaigh, C. Ó., Stokes, C. R., Livingstone, S. J., and Hillenbrand, C. D.: Understanding controls on rapid ice-stream retreat during the last deglaciation of Marguerite Bay, Antarctica, using a numerical model, J. Geophys. Res-Earth, 119, 247–263, https://doi.org/10.1002/2013JF002934, 2014.

Jeffries, S.: KAGA Site Information https://www.unavco.org/instrumentation/networks/status/pbo/overview/KAGA, 2014.

Jenkins, A.: Convection-driven melting near the grounding lines of ice shelves and tidewater glaciers, J. Phys. Oceanogr., 41, 2279–2294, https://doi.org/10.1175/JPO-D-11-03.1, 2011.

Jóhannesson, T., Raymond, C. F., and Waddington, E. D.: A Simple Method for Determining the Response Time of Glaciers, Glac. Quat. G., 6, 343–352, https://doi.org/10.1007/978-94-015-7823-3, 1989.

Joughin, I., Abdalati, W., and Fahnestock, M.: Large fluctuations in speed on Greenland's Jakobshavn Isbræ glacier, Nature, 432, 608–610, https://doi.org/10.1038/nature03130, 2004.

Joughin, I., Smith, B. E., Howat, I. M., Floricioiu, D., Alley, R. B., Truffer, M., and Fahnestock, M.: Seasonal to decadal scale variations in the surface velocity of Jakobshavn Isbrae, Greenland: Observation and model-based analysis, J. Geophys. Res-Earth, 117, 1–20, https://doi.org/10.1029/2011JF002110, 2012.

Joughin, I., Smith, B. E., Shean, D. E., and Floricioiu, D.: Brief Communication: Further summer speedup of Jakobshavn Isbræ, Cryosphere, 8, 209–214, https://doi.org/10.5194/tc-8-209-2014, 2014.

Joughin, I., Smith, B. E., and Howat, I. M.: A complete map of Greenland ice velocity derived from satellite data collected over 20 years, Journal of Glaciology, pp. 1–11, 2017.

Khan, S. A., Aschwanden, A., Bjørk, A. A., Wahr, J., Kjeldsen, K. K., and Kjær, K. H.: Greenland ice sheet mass balance: a review, Rep. Prog. Phys., 78, 046 801, https://doi.org/10.1088/0034-4885/78/4/046801, 2015.

Krabill, W.: Greenland Ice Sheet: High-Elevation Balance and Peripheral Thinning, Science, 289, 428–430, https://doi.org/10.1126/science.289.5478.428, 2000.

Lea, J. M., Mair, D. W. F., Nick, F. M., Rea, B. R., Van As, D., Morlighem, M., Nienow, P. W., and Weidick, A.: Fluctuations of a Greenlandic tidewater glacier driven by changes in atmospheric forcing: Observations and modelling of Kangiata Nunaata Sermia, 1859-present, Cryosphere, 8, 2031–2045, https://doi.org/10.5194/tc-8-2031-2014, 2014.

Lloyd, J., Moros, M., Perner, K., Telford, R. J., Kuijpers, A., Jansen, E., and McCarthy, D.: A 100 yr record of ocean temperature control on the stability of Jakobshavn Isbrae, West Greenland, Geology, 39, 867–870, https://doi.org/10.1130/G32076.1, 2011.

Long, A. J., Roberts, D. H., and Rasch, M.: New observations on the relative sea level and deglacial history of Greenland from Innaarsuit, Disko Bugt, Quaternary Res., 60, 162–171, https://doi.org/10.1016/S0033-5894(03)00085-1, 2003.

Luckman, A. and Murray, T.: Seasonal variation in velocity before retreat of Jakobshavn Isbræ, Greenland, Geophys. Res. Lett., 32, 1–4, https://doi.org/10.1029/2005GL022519, 2005.

Lüthi, M., Funk, M., Iken, A., Gogineni, S., and Truffer, M.: Mechanisms of fast flow in Jakobshavn Isbrae, West Greenland: Part III. Measurements of ice deformation, temperature and cross-borehole conductivityin boreholes to the bedrock, J. Glaciol., 48, 369–385, https://doi.org/10.3189/172756502781831322, 2002.

Moon, T., Joughin, I., Smith, B., and Howat, I.: 21st-Century Evolution of Greenland Outlet Glacier Velocities, Science, 336, 576–578, https://doi.org/10.1126/science.1219985, 2012.

Morlighem, M., Rignot, E., Mouginot, J., Seroussi, H., and Larour, E.: Deeply incised submarine glacial valleys beneath the Greenland ice sheet, Nat. Geosci., 7, 18–22, https://doi.org/10.1038/ngeo2167, 2014.

Morlighem, M., Bondzio, J., Seroussi, H., Rignot, E., Larour, E., Humbert, A., and Rebuffi, S.: Modeling of Store Gletscher's calving dynamics, West Greenland, in response to ocean thermal forcing, Geophysical Research Letters, 43, 2659–2666, 2016.

Motyka, R. J., Truffer, M., Fahnestock, M., Mortensen, J., Rysgaard, S., and Howat, I.: Submarine melting of the 1985 Jakobshavn Isbrae floating tongue and the triggering of the current retreat, J. Geophys. Res-Earth, 116, 1–17, https://doi.org/10.1029/2009JF001632, 2011.

Muresan, I. S., Khan, S. A., Aschwanden, A., Khroulev, C., Van Dam, T., Bamber, J., Broeke, M. R. V. D., Wouters, B., Kuipers Munneke, P., and Kjær, K. H.: Modelled glacier dynamics over the last quarter of a century at Jakobshavn Isbræ, Cryosphere, 10, 597–611, https://doi.org/10.5194/tc-10-597-2016, 2016.

Nick, F. M., Vieli, A., Howat, I. M., and Joughin, I.: Large-scale changes in Greenland outlet glacier dynamics triggered at the terminus., Nat. Geosci., 2, 110–114, https://doi.org/10.1038/ngeo394, 2009.

Nick, F. M., Van Der Veen, C. J., Vieli, A., and Benn, D. I.: A physically based calving model applied to marine outlet glaciers and implications for the glacier dynamics, J. Glaciol., 56, 781–794, https://doi.org/10.3189/002214310794457344, 2010.

Nick, F. M., Vieli, A., Andersen, M. L., Joughin, I., Payne, A., Edwards, T. L., Pattyn, F., and van de Wal, R. S. W.: Future sea-level rise from Greenland's main outlet glaciers in a warming climate., Nature, 497, 235–8, https://doi.org/10.1038/nature12068, 2013.

Nye, J.: The distribution of stress and velocity in glaciers and ice-sheets, P. Roy. Soc. Lond. A Mat., 239, 123–133, https://doi.org/10.1098/rspa.1957.0026, 1957.

Nye, J. F.: The Response of Glaciers and Ice-Sheets to Seasonal and Climatic Changes, P. Roy. Soc. Lond. A Mat., 256, 559–584, 1960.

Pollard, D., Deconto, R. M., and Alley, R. B.: Potential Antarctic Ice Sheet retreat driven by hydrofracturing and ice cliff failure, Earth Planet Sc. Lett., 412, 112–121, https://doi.org/10.1016/j.epsl.2014.12.035, 2015.

Reeh, N., Thomsen, H. H., Higgins, A. K., and Weidick, A.: Sea ice and the stability of north and northeast Greenland floating glaciers, Ann. Glaciol., 33, 474–480, https://doi.org/doi:10.3189/172756401781818554, 2001.

Rignot, E. and Kanagaratnam, P.: Changes in the Velocity Structure of the Greenland Ice Sheet, Science, 311, 986–990, https://doi.org/10.1126/science.1121381, 2006.

Rignot, E. and Mouginot, J.: Ice flow in Greenland for the International Polar Year 2008-2009, Geophys. Res. Lett., 39, 1–7, https://doi.org/10.1029/2012GL051634, 2012.

Robel, A. A.: Thinning sea ice weakens buttressing force of iceberg mélange and promotes calving, Nat. Commun., 8, 14 596, https://doi.org/10.1038/ncomms14596, 2017.

Schoof, C.: Ice sheet grounding line dynamics: Steady states, stability, and hysteresis, J. Geophys. Res-Earth, 112, 1–19, https://doi.org/10.1029/2006JF000664, 2007.

Schoof, C., Davis, A. D., and Popa, T. V.: Boundary layer models for calving marine outlet glaciers, Cyrosphere Discussions, pp. 1–30, https://doi.org/10.5194/tc-2017-42, 2017.

Sciascia, R., Straneo, F., Cenedese, C., and Heimbach, P.: Seasonal variability of submarine melt rate and circulation in an East Greenland fjord, J. Geophys. Res-Oceans, 118, 2492–2506, https://doi.org/10.1002/jgrc.20142, 2013.

Shapero, D. R., Joughin, I. R., Poinar, K., Morlighem, M., and Gillet-Chaulet, F.: Basal resistance for three of the largest Greenland outlet glaciers, J. Geophys. Res-Earth, 121, 168–180, https://doi.org/10.1002/2015JF003643, 2016.

Sohn, H., Jezek, K. C., and van der Veen, C. J.: Jakobshavn Glacier, west Greenland: 30 years of spaceborne observations, Geophys. Res. Lett., 25, 2699–2702, https://doi.org/10.1029/98GL01973, 1998.

Sole, A. J., Mair, D. W. F., Nienow, P. W., Bartholomew, I. D., King, M. A., Burke, M. J., and Joughin, I.: Seasonal speedup of a Greenland marine-terminating outlet glacier forced by surface melt-induced changes in subglacial hydrology, J. Geophys. Res-Earth, 116, 1–11, https://doi.org/10.1029/2010JF001948, 2011.

Straneo, F. and Cenedese, C.: The Dynamics of Greenland's Glacial Fjords and Their Role in Climate, Review of Marine Science, 7, 89–112, https://doi.org/10.1146/annurev-marine-010213-135133, 2015.

Straneo, F. and Heimbach, P.: North Atlantic warming and the retreat of Greenland's outlet glaciers., Nature, 504, 36–43, https://doi.org/10.1038/nature12854, 2013.

Straneo, F., Heimbach, P., Sergienko, O., Hamilton, G., Catania, G., Griffies, S., Hallberg, R., Jenkins, A., Joughin, I., Motyka, R., Pfeffer, W. T., Price, S. F., Rignot, E., Scambos, T., Truffer, M., and Vieli, A.: Challenges to understanding the dynamic response of Greenland's marine terminating glaciers to oc eanic and atmospheric forcing, B. Am. Meteol. Soc., 94, 1131–1144, https://doi.org/10.1175/BAMS-D-12-00100.1, 2013.

Streuff, K., Cofaigh, C. Ó., Hogan, K., Jennings, A., Lloyd, J. M., Noormets, R., Nielsen, T., Kuijpers, A., Dowdeswell, J. A., and Weinrebe, W.: Seafloor geomorphology and glacimarine sedimentation associated with fast-flowing ice sheet outlet glaciers in Disko Bay, West Greenland, Quaternary Sci. Rev., 169, 206–230, 2017.

Tedstone, A. J., Nienow, P. W., Gourmelen, N., Dehecq, A., Goldberg, D., and Hanna, E.: Decadal slowdown of a land-terminating sector of the Greenland Ice Sheet despite warming, Nature, 526, 692–695, https://doi.org/10.1038/nature15722, 2015.

Thomas, R. H., Abdalati, W., Frederick, E., Krabill, W. B., Manizade, S., and Steffen, K.: Investigation of surface melting and dynamic thinning on Jakobshavn Isbræ, Greenland, J. Glaciol., 49, 231–239, https://doi.org/10.3189/172756503781830764, 2003.

van der Veen, C. J.: Tidewater calving, J. Glaciol., 42, 375–385, https://doi.org/10.1179/102453311X13127324303399, 1996.

van der Veen, C. J.: Fracture propagation as means of rapidly transferring surface meltwater to the base of glaciers, Geophys. Res. Lett., 34, 1–5, https://doi.org/10.1029/2006GL028385, 2007.

van der Veen, C. J. and Whillans, I. M.: Model experiments on the evolution and stability of ice streams, Ann. Glaciol., 23, 129–137, 1996.

Vieli, A. and Nick, F. M.: Understanding and Modelling Rapid Dynamic Changes of Tidewater Outlet Glaciers: Issues and Implications, Surv. Geophys., 32, 437–458, https://doi.org/10.1007/s10712-011-9132-4, 2011.

Vieli, A. and Payne, A. J.: Assessing the ability of numerical ice sheet models to simulate grounding line migration, J. Geophys. Res-Earth, 110, 1–18, https://doi.org/10.1029/2004JF000202, 2005.

Vieli, A., Funk, M., and Blatter, H.: Flow dynamics of tidewaterg laciers: A numerical modelling approach, J. Glaciol., 47, 595–606, https://doi.org/10.3189/172756501781831747, 2001.

Warren, C. R.: Terminal environment, topographic control and fluctuations of West Greenland glaciers, 20, 1–15, 1991.

Weertman, J.: Stability of the junction of an ice sheet and an ice shelf, J. Glaciol., 13, 3–11, 1974.

Weidick, A. and Bennike, O.: Quaternary glaciation history and glaciology of Jakobshavn Isbrae and the Disko Bugt region, West Greenland: a review, Geol. Surv. Den. Greenl., p. 78, 2007.

Xu, Y., Rignot, E., Menemenlis, D., and Koppes, M.: Numerical experiments on subaqueous melting of greenland tidewater glaciers in response to ocean warming and enhanced subglacial discharge, Ann. Glaciol., 53, 229–234, https://doi.org/10.3189/2012AoG60A139, 2012.

Xu, Y., Rignot, E., Fenty, I., Menemenlis, D., and Flexas, M. M.: Subaqueous melting of Store Glacier, west Greenland from three-dimensional, high-resolution numerical modeling and ocean observations, Geophys. Res. Lett., 40, 4648–4653, https://doi.org/10.1002/grl.50825, 2013.